Performance Comparison of Two Commercial Small Animal PET Scanners: ClearPET™ and rPET-1™

Mario Cañadas, Miguel Embid, Eduardo Lage, *Member, IEEE*, Manuel Desco, Juan José Vaquero, *Senior Member, IEEE* and José Manuel Pérez, *Member, IEEE*

***Abstract*– It is usually difficult to compare different designs of Positron Emission Tomography (PET) small-animal scanners because of the disparity of measurements protocols. In this work we compare two commercial PET scanners installed at CIEMAT (Madrid, Spain): the ClearPET and the rPET-1, using an assessment procedure that fulfilled the recommendations of the new NEMA NU 4-2008 standard to evaluate small animal PET systems, including spatial resolution, sensitivity, scatter fraction and count losses studies. The scanners evaluated have significant geometrical differences, like the axial field of view (110 mm on ClearPET versus 45.6 mm on rPET-1), the configuration of the detectors (one pair of planar blocks on rPET-1, versus whole ring detectors on ClearPET) and the use of an axial shift between ClearPET module detectors. Our experiments showed a FWHM (FOV center, averaged over the three axes) of 1.98 mm for the rPET-1 and 2.15 mm for the ClearPET, with a small variation across the transverse axis on both scanners (<1 mm). The absolute sensitivity was 1.0% per detector pair for rPET-1 and 4.7% for ClearPET. Regarding count losses studies, the obtained peak NEC rate is 73.4 kcps at 0.51 MBq/ml for the ClearPET and 29.2 kcps at 1.35 MBq/ml for the rPET-1, considering a NEMA mouse-like phantom.**

I. Introduction

SMALL animal Positron Emission Tomography (PET) is becoming an essential imaging modality for preclinical research [1] and in the search for new radiopharmaceuticals [2]. At same time, manufacturers of clinical PET systems use these scanners to test new developments from a technological point of view.

The comparison and evaluation of different scanners must be carried out following the same conditions on issues like the image reconstruction protocol or the radioisotope used, which may change significantly the results. This is even more critical if the systems have different geometrical designs, like the two scanners that are considered in this work. The ClearPET (manufactured by Raytest GmbH [3]) is composed of a rotating full ring of detectors with an axial field of view (FOV) of 10.1 cm and a axial-shift of 9.2 mm between each two adjacent detectors, whereas the rPET-1 (manufactured by Suinsa Medical Systems, S.A. [4]) has two rotating planar block detectors and an axial FOV of 4.56 cm. Both use pixilated crystals: LYSO/LuYAP, phoswich matrix with two layers in the ClearPET [5] and MLS, one layer in the rPET-1 [6].

For the above reason, although performance characterization of both systems has been done separately [7] [8], the work presented here will compare them in the same conditions and following the recommendations of the new NEMA NU 4-2008 standard [9] created to evaluate small animal PET systems. The main interest of this work is to asses the influence of the design differences between these scanners, specifically the axial-shifted detectors [10] and the planar versus circular ring configuration.

II. Materials and Methods

All the measurements have been carried out on the scanners located at CIEMAT (*Centro de Investigaciones Energéticas, Medioambientales y Tecnológicas*), Madrid (Spain). Table I shows the geometrical and physical characteristics of both systems.

TABLE I
CHARACTERISTICS AND GEOMETRICAL DIMENSIONS OF THE CLEARPET AND THE RPET-1

Characteristics	ClearPET	rPET-1
Detector ring diameter (mm)	135 / 220	140
Number of module detectors	20	2
Number of PMTs (photomultiplier tubes)	80	2
Total PMTs sensitive area (cm^2)	262.1	48.0
Layers of crystals, radial direction	2	1
Crystal size (mm^3)	2x2x10	1.4x1.4x12
Total scintillator volume (cm^3)	409.6	42.3
Axial FOV (mm)	110	45.6
Maximum transversal FOV (mm)	94	45.6
Crystal material	LYSO / LuYAP	MLS
Rotating gantry	Yes	Yes

It is important to remark that the rPET-1 system considered is composed of only two block detectors, while other available versions of rPET systems have four blocks (two plus two placed in opposite positions). This will essentially affect the

Manuscript received November 14, 2008.

M. Canadas is with the CIEMAT (*Centro de Investigaciones Energéticas, Tecnológicas y Medioambientales)* Av. Complutense, 22, 28040 Madrid, Spain. (corresponding author phone: +34 91 3460872; fax: +34 91 3466275; e-mail: mario.canadas@ciemat.es).

M. Embid and J.M. Pérez are with the CIEMAT (*Centro de Investigaciones Energéticas, Tecnológicas y Medioambientales)* Av. Complutense, 22, 28040 Madrid, Spain.

E. Lage, M. Desco and J.J. Vaquero are with the *Unidad de Medicina y Cirugía Experimental, Hospital General Universitario Gregorio Marañón*, Madrid, Spain.

global sensitivity of the two-block system, being close to a half of the four-block version scanner. Another remarkable difference between them is that the rPET-1 incorporates a CT (Computed Tomography) system so that it can work as a PET/CT scanner. Referring to the ClearPET, its detector modules have the possibility to change the inner diameter from 13.5 cm to 22 cm, for mouse/rat or primate imaging purposes. This work is focused on the small diameter recommended to be used with mouse/rat. Regarding data processing, the main difference between these systems is that the rPET-1 processes counts in coincidences on-line, storing a list-mode file of coincidence events, whereas the ClearPET stores a list-mode file with the single photon energy depositions and the coincidence sorting is applied off-line after acquisition.

The methodology used to evaluate the performance of both scanners follows the recommendations of the new NEMA NU 4-2008 [9] standard. The protocol was recently approved by an international committee composed of different manufacturers of small animal PET systems, including the two considered here. The presented results include studies of:

- Spatial resolution
- Sensitivity
- Scatter fraction, count losses and random coincidence measurements

In addition, a micro Derenzo ^{22}Na sealed phantom was scanned and reconstructed on both systems. The acquisition of a Derenzo image, although it is not included on the NEMA protocol, is a common way to illustrate the spatial resolution of a scanner. Furthermore, the availability of a sealed phantom makes this measurement easily repeatable and comparable, without being affected by eventual bubbles that could appear in liquid-filled phantoms.

A. *Spatial Resolution*

A 0.25 mm diameter 0.8 MBq ^{22}Na point source was scanned at same positions on both scanners. The considered acquisition points are located at the axial center of FOV, and one-fourth of the axial center of FOV, at the following radial distances from center: 0 mm, 5 mm, 10 mm, 15 mm and 20 mm.

More than 10^5 prompt counts were acquired per measurement and analytic image reconstruction algorithms with no smoothing filters were considered on both scanners. Regarding the ClearPET, a direct 3D Filtered Back Projection (3D-FBP) algorithm was used, whereas a Single Slice Rebinning (SSRB) following by 2D-FBP was the reconstruction applied on the rPET-1. The image pixel size was kept according to the manufacturer's recommendations for each scanner (1.15 mm for ClearPET, and 0.773 mm for rPET-1)

The reported values characterize the width of the reconstructed image point spread functions (PSF), defining the width as its full width at half-maximum amplitude (FWHM) and the full width at tenth-maximum amplitude (FWTM). The response function is formed by summing all one-dimensional profiles that are parallel to the direction of measurement (radial, tangential or axial) and within two times the FWHM of the orthogonal directions. The fitting method used to assess each FWHM (and FWTM) fulfills the indications of the NEMA NU 4-2008 protocol.

B. *Sensitivity*

Sensitivity is expressed as the rate, in counts per second, that true coincidence events are detected for a given source intensity and branching ratio; absolute sensitivity is the fraction of positron annihilation events detected as true coincidence events [7]. The same ^{22}Na point source described previously was scanned in small position increments along the entire axial FOV. According to the NEMA protocol, the considered increments must be identical to the reconstructed plane thickness (similar to the pixel size of each scanner).

The variables S_{tot}, SM_{tot}, SR_{tot} represent the *total*, *total mouse* (7 cm) and *total rat* (15 cm) axial length sensitivities. Their values are reported as well as the absolute sensitivities ($S_{A,tot}$, $SM_{A,tot}$, $SR_{A,tot}$) and the sensitivity profiles by plotting the absolute sensitivity for each slice.

C. *Scatter Fraction*

A NEMA mouse-like phantom was fabricated to be used on these studies. The phantom is made of a solid cylinder composed of high-density polyethylene (density 0.95 g/cm^3) 70 mm long and 25 mm in diameter. A cylindrical hole (3.2 mm diameter) is drilled parallel to the central axis at the radial distance of 10 mm. A line source is inserted in the hole, made of a flexible tubing of 60 mm filled with a known activity of ^{18}F solution and positioned in the center of FOV as shown on Fig. 1.

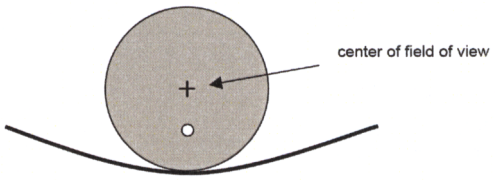

Fig. 1. Positioning of the NEMA mouse-like phantom. Image taken from [7].

Data processing is defined in the NEMA NU 4-2008 and it was applied at same level on both scanners. The acquisition started after the count rate measurements (see next section) using the same set-up at a sufficiently low counting rate such that random coincidences, deadtime effects and pileup are negligible.

D. Count Rates

Count rates and count losses measurements show the effects of system dead-time and the generation of random coincidence events at several levels of source activity. They were carried out using the same mouse-like phantom defined in the previous section, performing a dynamic study that starts with high activity, exceeding the expected upper count rate on both scanners, and stores the prompt, random and scattered coincidences as a function of time.

The considered NEMA protocol defines the procedure to classify random and scattered counts. Using the scatter fraction (SF) information it is possible to assess a Noise Equivalent Counts (NEC) rate whose peak shows an estimation of the maximum coincidences rate reached by the system exempt of scattered and random coincidences, defined as:

$$R_{NEC,i,j} = \frac{R_{t,i,j}^2}{R_{TOT,i,j}} \quad (1)$$

where $R_{NEC,i,j}$ $R_{t,i,j}$ and $R_{TOT,i,j}$ are the *NEC*, *trues* and *total* count rates for each acquisition j and slice i (counts are obtained from the 2D sinogram of each axial slice that is formed after SSRB rebinning, see details in NEMA, section 4 [7]). *Total* counts (also known as *prompts*) are referred to the total valid coincidences stored by the system whereas *true* counts are estimated as the total counts minus the scattered and random coincidences.

The above equation is valid for systems without direct random event subtraction, as the two considered here. The estimation of the random events is done as follows:

$$R_{r,i,j} = R_{TOT,i,j} - \frac{R_{t,i,j}}{1 - SF_i} \quad (2)$$

Nevertheless, in the case of ClearPET, it is possible to include a random subtraction method, based on shifted coincidence windows, that is applied off-line. Regarding natural radioactivity in the crystal, the rPET-1 presents a negligible intrinsic random count rate (less than 10 cps, according to the manufacturer) whereas the ClearPET reaches an intrinsic rate around 560 cps which was included in the assessment of scatter fraction and count rates. The intrinsic count rate of the ClearPET was obtained from an acquisition using the same phantom without activity.

The reported results include a plot with the true, random, scattered, NEC and total count rate (kcps) as a function of the average effective activity concentration (MBq/ml, where the volume considered is the total volume of the mouse-like phantom: 34.4 ml). The peak true count rate, $R_{t,peak}$, the peak NEC rate $R_{NEC,peak}$ and the activity concentration at which they are reached ($a_{t,peak}$, $a_{NEC,peak}$) are also presented for both scanners. The acquisition frames (j) were selected as follows: frames of 800 seconds starting each 1600 seconds for the rPET-1; and frames of 300 seconds starting each 1200 seconds for the ClearPET. In both cases, the radioisotope used was a solution of ^{18}F and the measurements were performed at intervals more frequent than half the radionuclide half-life, 3294 s. The initial amount of activity was 1.24 MBq/ml (1153.9 uCi total activity) for ClearPET and 1.61 MBq/ml (1491.7 uCi) for rPET-1.

E. Derenzo phantom images

Acquisition of a Derenzo image is not included on the NEMA protocol; nevertheless it is an intuitive way to illustrate the spatial resolution and assess the image quality of a scanner. The phantom presented a total activity of 1MBq of ^{22}Na on July 15th 2007. It is composed of 20 rods of 1.2 mm diameter, 14 rods of 1.5 mm, 9 rods of 2.0 mm, 6 rods of 2.5 mm and 3 rods of 3.0 mm. The rods of equal diameter are distant from each other by twice the diameter of the rods, center to center. The external dimensions of the phantom are 43 mm length by 40 mm diameter.

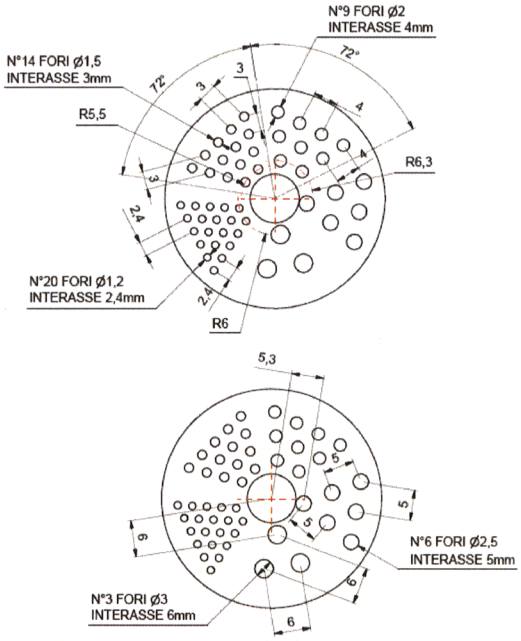

Fig. 2. Dimensions of the micro Derenzo phantom.

III. Results

A. Spatial Resolution

At center of FOV, the average one dimensional FWHM over the three axes is 1.98 mm (FWTM: 4.08 mm) in the rPET-1 and 2.15 mm (FWTM: 4.69 mm) in the ClearPET. Resolution over the same transaxial points has been also assessed at ¼ axial FOV finding no significant differences with the values showed at axial center FOV, specifically the average one dimensional FWHM over the three axes at transaxial center at

¼ axial FOV is 1.90 mm (FWTM: 4.05 mm) in the rPET-1 and 2.19 mm (FWTM: 4.58 mm). Table II shows a report following the NEMA NU 4-2008 format, with the results of spatial resolution obtained on both systems.

TABLE II
NEMA SPATIAL RESOLUTION OF THE CLEARPET AND THE RPET-1

ClearPET

Reconstructed image pixel size (mm): **1.150**								
Slice thickness (mm): **1.150**								
At axial center								
	5 mm		10 mm		15 mm		20 mm	
	FWHM	FWTM	FWHM	FWTM	FWHM	FWTM	FWHM	FWTM
Radial	**2.35**	**4.60**	**1.81**	**3.95**	**2.31**	**4.19**	**2.73**	**4.81**
Tangential	**2.30**	**4.58**	**2.65**	**6.64**	**2.77**	**5.87**	**2.50**	**4.98**
Axial	**3.23**	**6.03**	**3.15**	**5.87**	**3.18**	**5.91**	**3.18**	**5.89**
At 1/4 axial FOV from center								
	5 mm		10 mm		15 mm		20 mm	
	FWHM	FWTM	FWHM	FWTM	FWHM	FWTM	FWHM	FWTM
Radial	**2.32**	**4.75**	**1.98**	**4.20**	**2.21**	**4.20**	**2.84**	**4.79**
Tangential	**2.40**	**4.65**	**2.59**	**5.69**	**2.69**	**5.47**	**2.57**	**5.12**
Axial	**3.16**	**5.86**	**3.16**	**5.77**	**3.17**	**5.75**	**3.17**	**5.75**

rPET-1

Reconstructed image pixel size (mm): **0.773**								
Slice thickness (mm): **0.773**								
At axial center								
	5 mm		10 mm		15 mm		20 mm	
	FWHM	FWTM	FWHM	FWTM	FWHM	FWTM	FWHM	FWTM
Radial	**1.52**	**3.14**	**1.45**	**2.81**	**1.21**	**2.60**	**1.36**	**2.15**
Tangential	**1.84**	**4.05**	**2.02**	**4.71**	**2.30**	**6.25**	**2.69**	**8,43**
Axial	**2.57**	**4.84**	**2.78**	**5.40**	**3.12**	**5.96**	**2.92**	**6.13**
At 1/4 axial FOV from center								
	5 mm		10 mm		15 mm		20 mm	
	FWHM	FWTM	FWHM	FWTM	FWHM	FWTM	FWHM	FWTM
Radial	**1.59**	**3.49**	**1.58**	**3.16**	**1.58**	**2.79**	**1.52**	**2.75**
Tangential	**1.80**	**3.59**	**1.83**	**3.70**	**1.93**	**4.52**	**1.96**	**4.69**
Axial	**2.41**	**4.89**	**2.83**	**5.12**	**3.38**	**5.64**	**3.42**	**5.97**

The spatial resolution (FWHM) obtained at axial center FOV across transaxial axis is presented in Fig. 3a and 3b. Both scanners show a small variation on the average FWHM across the transverse axis (less than 1 mm) that is achieved by different solutions in each scanner: ClearPET uses two layers of crystals to asses the depth of interaction (DOI) of the incoming photon on the detectors, minimizing the parallax error; whereas rPET-1 uses planar opposite detectors, so that most of the incoming photons have parallel trajectories within the pixelated crystals.

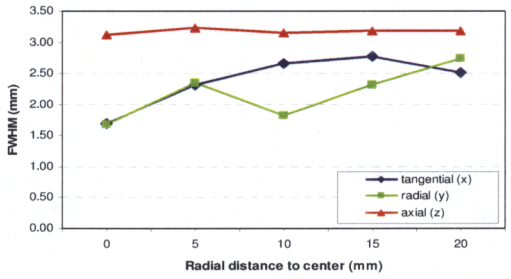

Fig. 3a. ClearPET NEMA spatial resolution (FWHM) at axial center of FOV.

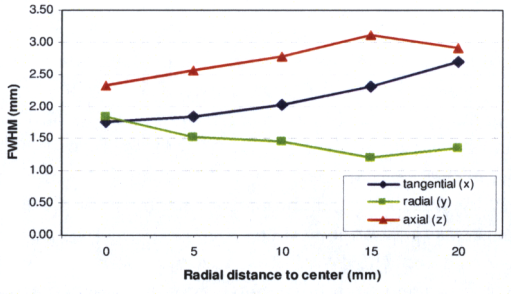

Fig. 3b. rPET-1 NEMA spatial resolution (FWHM) at axial center of FOV.

The average, minimum and maximum FWHM over the three directions on both scanners are plotted for each transaxial point in Fig. 4. Except for transaxial center of FOV, rPET-1 shows approximately 0.5 mm better averaged spatial resolution than ClearPET on the transaxial points measured.

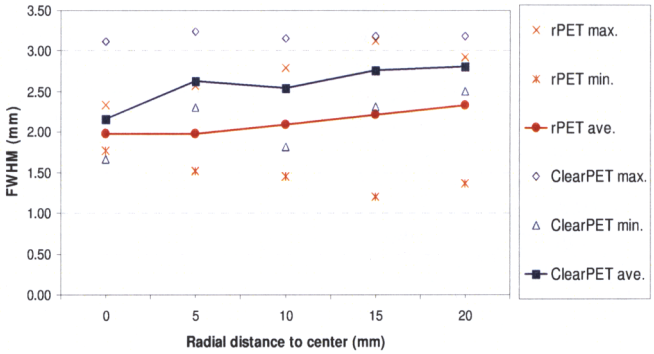

Fig. 4. ClearPET versus rPET-1 spatial resolution at axial center of FOV. Average, minimum and maximum FWHM over the three axis profiles.

B. Sensitivity

The absolute peak sensitivity obtained at the center of FOV is 1.0% for rPET-1 and 4.7% for ClearPET, considering a wide energy window: 100-700 keV. Table III shows the *total length* (S_{tot}) and *mouse length* (SM_{tot}) sensitivity values according to NEMA protocol. In the case of rPET-1 the S_{tot} and SM_{tot} values are identical because the axial extent of the system is lower than the length considered for mouse studies (7 cm). On both scanners the *rat length* sensitivity (SR_{tot}) is identical to the respective *total length* sensitivity. The low energy threshold selected was the same on both systems, 250 keV, which is the operational value recommended by the manufacturer.

TABLE III
NEMA SENSITIVITY RESULTS ON THE CLEARPET AND THE RPET-1

	ClearPET	rPET-1
$S_{A,tot}$ (%)	1.87	0.46
$SM_{A,tot}$ (%)	2.32	0.46
S_{tot} (kcps/MBq)	16.98	4.18
SM_{tot} (kcps/MBq)	21.08	4.18

Fig. 5 plots the NEMA absolute sensitivity profile as function of the axial distance to the center FOV in millimeters. An important difference between the systems is that ClearPET presents a 9.2 mm axial shift between adjacent radial detectors, the axial shifted detectors produce a less homogeneous profile than the rPET-1, whereas the axial FOV is enlarged with no empty sinograms (all axial slices are covered by detectors). In that case a specific normalization procedure it is required to compensate the lack of homogeneity across the axial axis of the ClearPET [11].

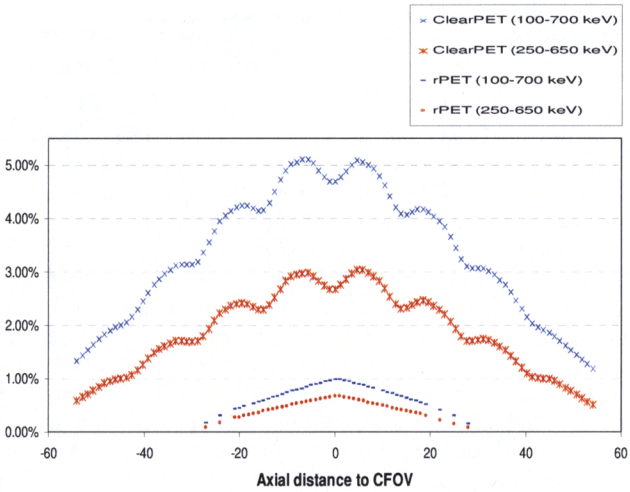

Fig. 5 ClearPET and rPET-1 absolute sensitivity profiles for two energy windows.

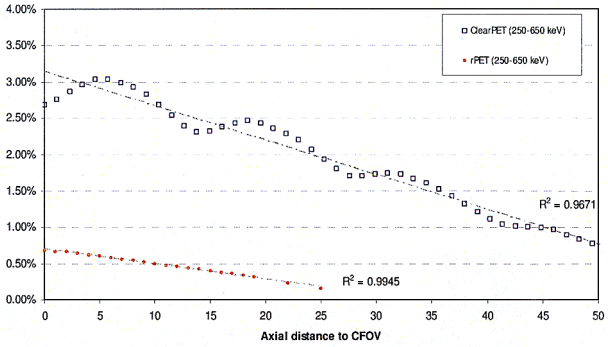

Fig. 6 Sensitivity profile homogeneity on the rPET-1 and ClearPET. Operational energy windows (250 -650 keV).

C. *Scatter Fraction*

The SF values obtained on each system were: 31.03 % for the ClearPET and 24.19 % for the rPET-1, considering the mouse-like phantom.

According to NEMA, the scattered counts include all the coincidences out of a 14 mm central strip on the source activity profile obtained shifting and integrating the rebinned sinograms over the axial axis. The acquisition was performed at a low enough activity so that the random event rate is less than 1% of true rate. It is important to remark that the rPET-1 axial FOV is close to 2 cm shorter than the active line source, whereas the line source is totally cover by detectors in the case of ClearPET (110 mm axial FOV)

D. *Count Rates*

The results of count rates are related to the mouse-like phantom (V= 34.4 ml). Fig. 7a and 7b show the total, trues, random, scattered and NEC count rates as function of the average activity concentration in the phantom for the ClearPET and the rPET-1, respectively.

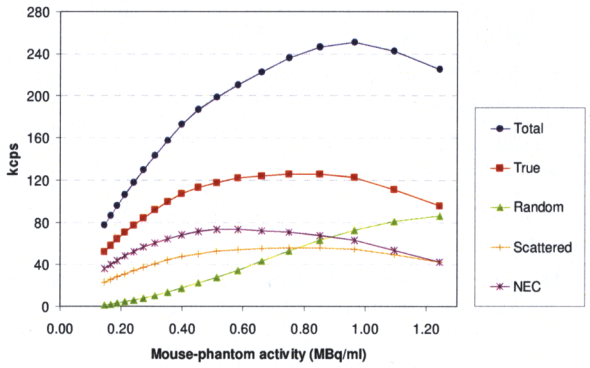

Fig. 7a. Total, trues, random, scattered and NEC count rates as function of the average activity in the mouse-like phantom for the ClearPET.

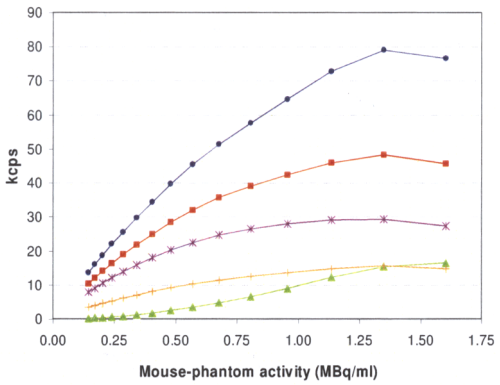

Fig. 7b. Total, trues, random, scattered and NEC count rates as function of the average activity in the mouse-like phantom for the rPET-1.

Table IV summarizes the peak NEC and true count rate reached on each scanner and the corresponding activity in the phantom. The higher count rate peaks reached on the ClearPET are explained by the different sensitivity of the systems. The lower sensitivity of the rPET-1 also contributes to the fact that the scanner reaches its peak with more activity in the phantom. Although the energy window chosen on both scanners was the same (250-650 keV), a comprehensive analysis of these results must also take into account the significantly different way of how the scanners process the data: the ClearPET system stores all the singles events on the hard disk of the preprocessor PC following a list-mode format in order to sort the coincidences off-line, whereas rPET-1 is storing coincidences on-line following also a list-mode format but with coincidence events.

TABLE IV
NEMA COUNT RATE RESULTS ON THE CLEARPET AND THE RPET-1

	ClearPET	rPET-1
$R_{trues,peak}$ (kcps)	126.0	78.9
$R_{NEC,peak}$ (kcps)	76.4	29.2
$a_{trues,\ peak}$ (MBq/ml)	0.75	1.35
$a_{NEC,\ peak}$ (MBq/ml)	0.51	1.35

E. Derenzo phantom images

The presented Derenzo images (Fig. 8) were reconstructed with iterative algorithms (OSEM) in both cases and parameters like the number of subsets or iterations were selected following the recommendations of the manufacturer of each system in order to obtain the best image quality.

It is possible to resolve the smallest rods (1.2 mm) only in the rPET-1 image, which is consistent with the spatial resolution results previously presented that show a better performance of the rPET-1 scanner using analytic reconstruction. Nevertheless, it is important to take into account that we are comparing images reconstructed with approximately the same number of counts but the acquisition time is close to five times higher on the rPET-1 than on the ClearPET, due to the different sensitivity of the systems.

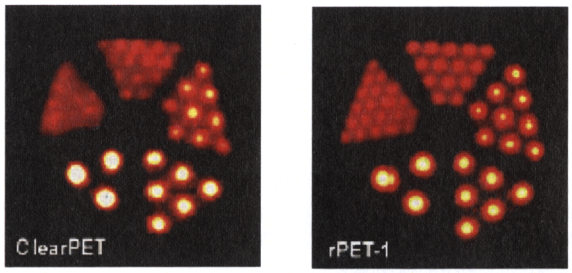

Fig. 8. Derenzo phantom scanned on the ClearPET and the rPET-1. Transaxial image, integrated over slices, after iterative reconstruction (OSEM)

IV. CONCLUSIONS

In this work we have presented an evaluation of two scanners following the new NEMA NU 4 – 2008 protocol for small PET systems. The results allow the comparison of both scanners under the same conditions in terms of spatial resolution, sensitivity, scatter fraction and count rates.

Regarding spatial resolution, both scanners show a good performance at the center of FOV and a small variation across the transaxial axis, less than 1 mm, with an average FWHM at CFOV: 1.98 mm for the rPET-1 and 2.15 for the ClearPET. Absolute sensitivity at the center of FOV is five times higher for the ClearPET, as expected from the different geometrical design and the use of close to ten times more active scintillator volume than the rPET-1.

Considering the NEMA mouse-like phantom, the measured scatter fraction was 31.03% in the ClearPET and 24.19 % in the rPET-1. Related to the same phantom, the peak NEC rate reaches 73.4 kcps at 0.51 MBq/ml in the ClearPET and 29.2 kcps at 1.35 MBq/ml in the rPET-1.

The overall performance shows that both the ClearPET and the rPET-1 systems are very suitable for preclinical research and imaging of rodent-sized animals.

REFERENCES

[1] G. D. Hutchins, M. A. Miller, V. C. Soon and T. Receveur, "Small animal PET imaging," *ILAR Journal (National Research Council, Institute of Laboratory Animal Resources)*, vol. 49, no. 1, pp. 54-65, 2008.

[2] T. J. McCarthy, "Positron emission tomography imaging as a key enabling technology in drug development," *Ernst Schering Res Found Workshop*, vol. 62, no. 3, pp. 29-39, 2007.

[3] Raytest Isotopenmessgeraete GmbH. Benzstraße 4. D-75334 Straubenhardt. Registrar: HRB 501307 in Mannheim, Germany. http://www.raytest.com/

[4] Suinsa S.A. C/ Primavera 39. Torrejón de Ardoz, 28850, Madrid, Spain. http://www.suinsa.com/

[5] J. B. Mosset, O. Devroede, M. Krieguer, M. Rey et al., "Development of an optimised LSO/LuYAP phoswich detector head for the ClearPET camera," *IEEE NSS 2005 Conf. Rec.* vol. 3, pp, 1641-1644, Oct. 2005.

[6] J. J Vaquero, E. Lage, L. Ricon, M. Abella, E. Vicente and M. Desco, "rPET detectors design and data processing," *IEEE NSS 2005 Conf. Rec.* vol. 5, pp. 2885-2889, Oct. 2005.

[7] P. Sempere Roldan, M. Canadas, O. Dietzel, C. Pautrot, I. Sarasola, A. Wagner, "Performance evaluation of Raytest ClearPET, a PET scanner for small and medium size animals," *IEEE NSS 2007 Conf. Rec.* vol. 4, pp. 2859-2864, Oct. 2007.

[8] E. Vicente, J. J. Vaquero, E. Lage, G. Tapias, M. Abella, J. L. Herráiz, S. España, J.M. Udías and M. Desco. "Caracterización del Tomógrafo de Animales rPET," (*In spanish*). *XXIV Annual Congress of the Spanish Society of Biomedical Engineering,* 2006. ISBN: 84-9769-160-1.

[9] National Electrical Manufacturers Association. Performance Measurements for Small Animal Positron Emission Tomographs (PETs). Rosslyn, VA; 2008. Standars Publication NU 4 – 2008 http://www.nema.org/stds/nu4.cfm

[10] U. Heinrichs, U. Pietrzyk and K. Ziemons "Design Optimization of the PMT-ClearPET Prototypes Based on simulation With GEANT3," *IEEE Trans. Nucl. Sci.* vol. 50, no. 5, pp. 1428-1432, Oct. 2003.

[11] S. Weber, B. Gundlich and M. Khodaverdi, "Normalization factors for the ClearPET Neuro," *IEEE NSS 2005 Conf. Rec.* vol. 5, pp. 2632-2635, Oct. 2005.